This manuscript is currently under peer review at the *Proceedings of the National Academy of Sciences* (PNAS).

Water-mediated hydrogen bonds and local side chain interactions in the cooperative collapse and expansion of PNIPAM oligomers

Wanlin Chen,[†] Martin Gruebele,[‡*] Martina Havenith,[†*] Kurt J. Hebel,[&] Carla Scaletti[&*]

[†]Physical Chemistry II, Faculty of Chemistry and Biochemistry, Ruhr University Bochum, Bochum, Germany.

[‡]Department of Chemistry, Department of Physics, and Center for Biophysics and Quantitative Biology, University of Illinois Urbana-Champaign, Illinois, USA.

[&]Symbolic Sound Corporation, Champaign, Illinois, USA.

[*]Corresponding authors: Martin Gruebele (mgruebel@illinois.edu); Martina Havenith (Martina.Havenith@ruhr-uni-bochum.de); Carla Scaletti (carla@symbolicsound.com)

Keywords: Water-mediated interactions, polymer compactification, cavity wrap water, bound water, sonification

Abstract

Poly(N-isopropylacrylamide) (PNIPAM), a thermoresponsive homopolymer, is a well-established model for investigating coil-to-globule transitions. Here, we combine long molecular dynamics (MD) simulations, data sonification, and graph-theory analysis to elucidate the roles of intramolecular and PNIPAM–solvent hydrogen-bond (H-bond) patterns in the PNIPAM globule-coil equilibrium. Our analysis separates the driving forces for compaction into two contributions: the entropic gain from the loss of hydration water around hydrophobic patches, and the enthalpic stabilization from water H-bonded to PNIPAM. We find that the role of the solvent in polymer compaction is more active and complex than has been previously assumed. Our observations indicate that direct, intra-chain hydrogen bonds between amide groups (N-H···O=C) are not the primary stabilizing force. Instead, the collapsed globule contains an N-H···N network of local side chain interactions and is stabilized by a dynamic network of persistent, long-distance water bridges, where individual water molecules form hydrogen bonds with multiple parts of the polymer chain.

Significance Statement

Materials that change shape with temperature are foundational for applications ranging from controlled drug release to soft robotics. Through computational simulations of how a model polymer collapses in water, we show that water is an active participant in this process by forming structural water bridges that pull the polymer into its compact state. The method developed here for analyzing hydrogen bond dynamics using auditory analytics — data analytics that combines mapping data to sound (sonification) and graphics (visualization) — provides new insights needed to decipher the complex dynamics typical of high-dimensional chemical and biological systems.

Introduction

Poly(N-isopropylacrylamide), or PNIPAM, is a homopolymer frequently employed in the synthesis of temperature-sensitive hydrogels with good mechanical properties;[1] it is often used as a model system for studying coil-to-globule transitions at a lower critical solution temperature (LCST).[2] A simple picture for polymer compaction upon heating is the increasing entropic driving force at higher temperature,[3] leading to the release of hydration water around hydrophobic patches.[4] Thus the transition is sensitive to solvent composition.[5,6] However, hydrogen bonding also plays an important role in the formation of compact polymer globules and their structural organization.[7]

Aqueous PNIPAM has been extensively investigated by experiment and molecular dynamics simulation. The latter work has led to improvements in simulated transition temperatures,[8] confirmed that PNIPAM tacticity has only a small effect on globule structure,[9] measured diffusion of water within the polymer matrix,[10] and looked at the effects of osmolytes,[11] among many other interesting properties. In a classic study, Tamai, Tanaka and Nakanishi studied hydrogen bonding of water near the PNIPAM surface,[12] but surprisingly little has been done since then to see how water-PNIPAM hydrogen bonds foster the transition from extended to compact states above the LCST.

Here we use long molecular dynamics simulations (cumulative 16 μs) to study the changes in hydrogen bonding during the cooperative passages of PNIPAM through the transition state ensemble as the oligomer switches between extended coil and compact globule states. We investigate a 30-mer of NIPAM in aqueous solution in equilibrium near the transition temperature, as it has been shown that cooperativity occurs for sizes < 60 kDa (<539 subunits).[13] We are able to observe multiple rapid coil-globule and globule-coil transitions in the simulation, as well as a population of long-lived intermediate compactness states. Not all transitions are fast compared to the dwell times in the coil and globule states because PNIPAM lacks any sequence-specific cooperativity, but we emphasize the subset of cooperative transitions between pairs of structurally distinct states here.

We combined sonification[14,15] and visualization tools with a 2D reaction coordinate space derived via dimensionality reduction to track complex H-bonding dynamics. The influence of direct polymer−polymer hydrogen bonds (DBs) on the dynamics of the polymer chain is less significant[16] than had been widely assumed. We find instead that the efficient collapse of PNIPAM is enabled by a combination of water-mediated hydrogen bonds (WBs) and amide-amide side chain interactions (SCBs) characterized by a specific N-H···N structure, with most transition state passages in the 2-3 ns range. Nonetheless, DB and WB H-bonding frequently traps PNIPAM in states of intermediate compactness that can persist for over 50 ns. As expected from the force field-dependent persistence length of PNIPAM (1-3 nm),[17] we observe compact states with one to five kinks in the polymer chain. We investigated correlations between DBs, WBs, and SCBs before, during, and after transition state passage between globule and coil forms of the PNIPAM oligomer.

Methods

Simulation details. The simulation system consists of a single PNIPAM polymer chain solvated in 32578 water molecules within a cubic box of approximately 10 × 10 × 10 nm³. The initial PNIPAM configuration was taken from the Supporting Information of Ref. [18]. A modified OPLS-AA force field

proposed by Mochizuki et al.,[19] which scales partial charges by a factor of 1.31, was used to model PNIPAM, combined with the SPC/E model[20] for water. This modified force field more accurately reproduces the demixing temperature in concentrated solutions and the coil–globule transition temperature in dilute solutions compared to the original OPLS-AA model.[16]

All simulations were performed using the GROMACS package.[21] The leapfrog algorithm with a 2 fs timestep was used for integration. Long-range electrostatics were treated with the particle mesh Ewald method, and a standard long-range correction was applied for Lennard–Jones interactions. Covalent bonds involving hydrogen in PNIPAM were constrained using LINCS,[22] while SETTLE[23] was used for water. Lorentz−Berthelot mixing rules were applied to determine the interaction between different atom types. Simulations were run in the NPT ensemble at 1 atm and 310 K using the Nosé–Hoover thermostat[24,25] and Parrinello–Rahman barostat.[26] After energy minimization and 20 ns equilibration, 11 independent production runs were conducted, with in total ~16 μs of simulation time.

Hydrogen bonds—either between PNIPAM residues (N–H···O) or between PNIPAM and water—were defined based on geometric criteria: a donor–acceptor distance less than 3 Å and a donor–hydrogen–acceptor angle greater than 140°. Side-chain interactions (SCB) were identified based on a nitrogen–nitrogen (N···N) distance of less than 4 Å and a corresponding N–H···N angle between 70° and 110°.

Analysis details. We developed the Kinetic Transition Estimator (KiTE), an $O(k\,N \log N)$ algorithm (where N = number of data frames, k = number of states), and applied it to the raw R_g data to estimate the start times and durations of coil-globule transitions in the simulation. The transition durations identified by KiTE are related by a scale factor to the transit times found using the STaSI method with logistic fits.[27,28] Further details on the KiTE algorithm are available in the Supporting Information (**Figs. S1-S3** and text).

Collective variables were defined as follows:

$$R_g = \frac{1}{M}\sum_i m_i r_i^2 \quad , \qquad [1]$$

where R_g is the radius of gyration, M total PNIPAM mass, m_i individual atom masses, and r_i individual atom distances from the PNIPAM center of mass. The solvent-accessible surface area (SASA) was computed using the FreeSASA package,[29] as the van der Waals surface of the solute expanded by a spherical solvent probe (radius 0.14 nm) centered on each atom, with van der Waals radii taken from Bondi[30,31]. The resulting SASA values were then partitioned into contributions from hydrophilic (N and O) and hydrophobic (methyl C) residues to obtain the exposed polar (EPHIA) and nonpolar (EPHOA) surface areas, respectively.

Polymer hydration was characterized by identifying water molecules within the first solvation shell of PNIPAM, using the definitions of cavity 'wrap' and 'bound' water,[4,32–36] as showcased in ref. [36] for the glycerol/water system. Wrap water surrounds non-polar methyl groups (within 5.5 Å of a methyl carbon) without direct H-bonding to the polymer, forming a two-dimensional water–water HB network wrapped around the polymer. This network shows a characteristic THz signature at 150–160 cm^{-1} due to collective HB stretching, red-shifted relative to bulk water. Bound water forms direct H-bonds with

PNIPAM, defined as water whose oxygen lies within 3.5 Å of a PNIPAM nitrogen or oxygen atom, with THz signature in the librational frequency range (400–600 cm^{-1}).[4] The numbers of both 'wrap' and 'bound' water were normalized by the number of PNIPAM residue.

Principal component analysis was used to construct a minimal set of two reaction coordinates from the collective variables, using a weighted average window. Additional variables to describe trajectories in the state space of two reaction coordinates include speed (the time derivative of the state space trajectory to identify sudden changes in state) and total span (the sum of all bond spans n between side chains I and $i+n$ in a given state).

Hydrogen bond dynamics were studied using auditory analytics,[37,38] an approach that combines statistical methods with iterative mapping of data to auditory (sonification) and visual (visualization) parameters. The authors examined individual trajectories using an interactive piano roll, a sonification and visualization of bond formation with respect to time and residue number, displayed in conjunction with the trajectory through a 2D state space defined by the principal components of 3-7 reaction coordinates (described below).

Several parameters of the multimodal display, including bond type, sequence separation or 'span' (distance between donor and acceptor by residue number), sound parameter ranges, rate, and reaction coordinate, are adjustable in real time, allowing for the listener to focus on various aspects of the data. This tool was developed using the Kyma language[39] (a sound design framework written in the Smalltalk programming language[40]) and is an extension of tools developed for studying H-bond dynamics during the protein-folding reaction.[38] See the Supporting Information **Fig. S4**, **Fig. S9**, and text for additional details on data shaping, sound synthesis methods and parameter mapping.

To characterize the overall correlation of bond types with compactness of the polymer, histograms were created to show each bond type, color-coded by sequence distance, as a function of sequence position (residue number) and R_g. In addition, a graph with residues as nodes, and bonds as type-coded vertices between nodes was made to visualize bonding patterns between side chains. Finally, betweenness centrality was used to highlight which residues are 'central' to the network of bonds, i.e. are links with maximal number of connections to other residues by measuring the fraction of shortest paths passing through a given residue. The betweenness centrality of residue v is defined as:

$$C_B(v) = \sum_{s \neq v \neq t} \sigma_{st}(v)/\sigma_{st}\,, \qquad [2]$$

where σ_{st} is the total number of shortest paths between residues s and t, and $\sigma_{st}(v)$ is the number of those paths that pass through v. Residues with high betweenness centrality serve as central "hubs" in the bonding network.

Results

Transitions between coil and globule states. Our goal is to elucidate the hydrogen bonding and structural arrangements that occur when PNIPAM makes rapid cooperative transitions between collapsed globule and extended coil forms. To that end, we investigated the conformational transitions of a single PNIPAM 30-mer in water by performing 11 independent molecular dynamics (MD)

simulations totaling about 16 μs (**Fig. 1** and **SI Fig. S1**). The simulations employed a modified OPLS-AA force field[8,19] for PNIPAM in combination with SPC/E water. Systems were simulated in the NPT ensemble at 1 atm and 310 K using the Nosé–Hoover thermostat, with a cubic box of approximately 10 × 10 × 10 nm^3 to ensure sufficient bulk solvent and to avoid boundary effects where the polymer could interact with itself.

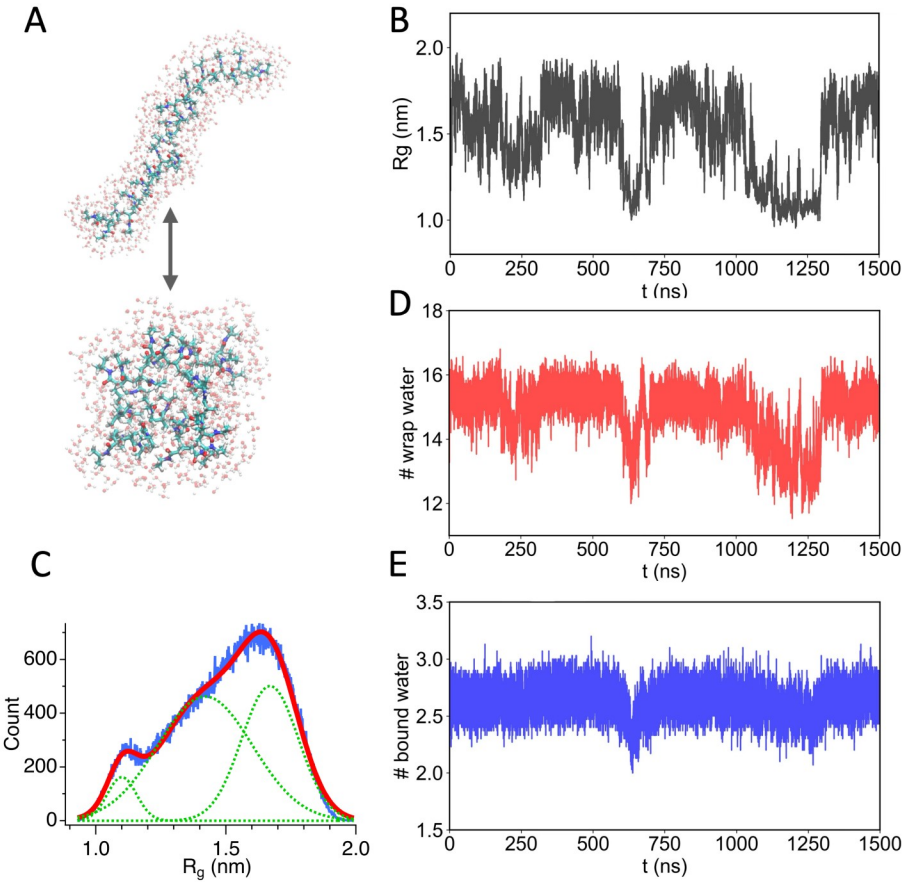

Fig. 1. A. Example of an extended (top) and compact (bottom) structure of PNIPAM. B. Radius of gyration (R_g) trajectory for one of the 11 simulation trajectories. C. Radius of gyration distribution (blue) and fit (red) to 3 Gaussian distributions, shown in green. D. Number of 'wrap water' molecules for the trajectory in B. E. Number of bound water molecules for the trajectory in B. **SI Fig. S1** shows all concatenated trajectories.

To estimate the probability of PNIPAM being in each of three states — coil, globule, and an intermediate ensemble of states — we modeled the radius of gyration (R_g) for all trajectories as three Gaussian distributions (**Fig. 1C and SI Table S1**). Not unexpectedly, the intermediate ensemble is highly populated (56%, vs. 7% for the globule and 37% for the coil state), indicating that PNIPAM's homopolymer collapse cannot be described by a simple two-state system although there are direct transitions between globule and coil states.

In our model, the globule and coil probabilities intersect at about 1.3 nm, in agreement with a previous simulation study of PNIPAM 40-mer[8] and a study of PNIPAM 30-mer where the globular state was defined as R_g<1.2 nm.[41] To identify the start times and durations of coil-globule transitions, we developed a Kinetic Transition Estimator algorithm (KiTE) and compared its results to those from

the Step Transition and State Identification STaSI algorithm[27]. Representative transitions identified by these methods are shown in SI **Tables S2** (KiTE) and **S3** (STaSI).

Direct passages between globule and coil with a confidence assigned by the KiTE estimator are shown in **SI Fig. S1A**. The histogram for all passages peaks in the 2-3 ns range, defining the 'speed limit' for full PNIPAM collapse (see histogram in **SI Fig. S3A** and **SI Tables S2 and S3**). These passage times are very similar to experimentally measured contact times for glycine oligomers of similar length (~5 ns).[42] The system shows some signs of cooperativity, with a mean dwell time (77 ns) in states that is roughly 16 times longer than the mean transit time (4.7 ns).

There are also many transitions where PNIPAM collapses into or escapes from partially compact traps whose lifetime exceeds 10 ns and that the oligomer has to escape before undergoing further collapse or expansion (examples in **SI Fig. S4**). These semi-compact trap states are consistent with the need to fit the R_g distribution to three Gaussians to obtain a reasonable fit (**Fig. 1C**); in the distribution in **SI Fig. S3A**, passages through intermediate states contribute to the tail at >10 ns, which is slower than the 'speed limit' peak of the distribution. Using the STaSI method (detailed in SI text) as an alternative to identify distinct states from R_g trajectories, trajectories were well described by a three-state model (coil, intermediate, and globule). Selected coil-to-globule transition passage times were quantified via logistic fits, yielding 26 events with transit times peaking at 2–3 ns (**Fig. S3B**), in agreement with the KiTE algorithm results (**Fig. S3A**).

To study the water dynamics and hydrogen bonding, we categorized the water molecules in PNIPAM's first solvation shell as either "wrap water" or "bound water" (see Methods). A classification previously established through Terahertz spectroscopy and molecular dynamics simulations of solvated polymers,[4] wrap water forms a hydrogen-bonded network around non-polar regions without directly H-bonding to the polymer, forming a two-dimensional water–water HB network wrapped around the solute, while bound water interacts with the polymer's polar groups.

In **Fig. 1D**, the number of wrap water molecules decreases as the polymer transitions from an extended to a compact state, closely mirroring the change in R_g. In contrast, the number of bound water molecules remains nearly constant during the simulation, although it is also weakly correlated with R_g. This behavior is consistent with findings from THz spectroscopy studies on liquid–liquid state separation (LLPS) of proteins, which suggest that the release of entropically unfavorable wrap water facilitates phase separation, whereas the retention of bound water reduces the enthalpic cost.[4]

Additional hydration-related properties such as the solvent-accessible surface area (SASA) for hydrophobic and hydrophilic residues, EPHOA (exposed hydrophobic area) and EPHIA (Exposed hydrophilic area = SASA-EPHOA), were computed to characterize changes in the polymer's exposure to water, and are discussed next in our analysis of transition state passage.

Transition state passage and reaction coordinate. To quantify transition state passage between extended and compact states,[43] we computed 5 coordinates for PNIPAM: R_g, EPHOA (exposed hydrophobic area), EPHIA (Exposed hydrophilic area), Wrap Water, and Bound Water, finding that two PCA components PC1 and PC2 extracted by singular value decomposition were sufficient to account for 93.5% of the variation in trajectories (**SI Table S4**).

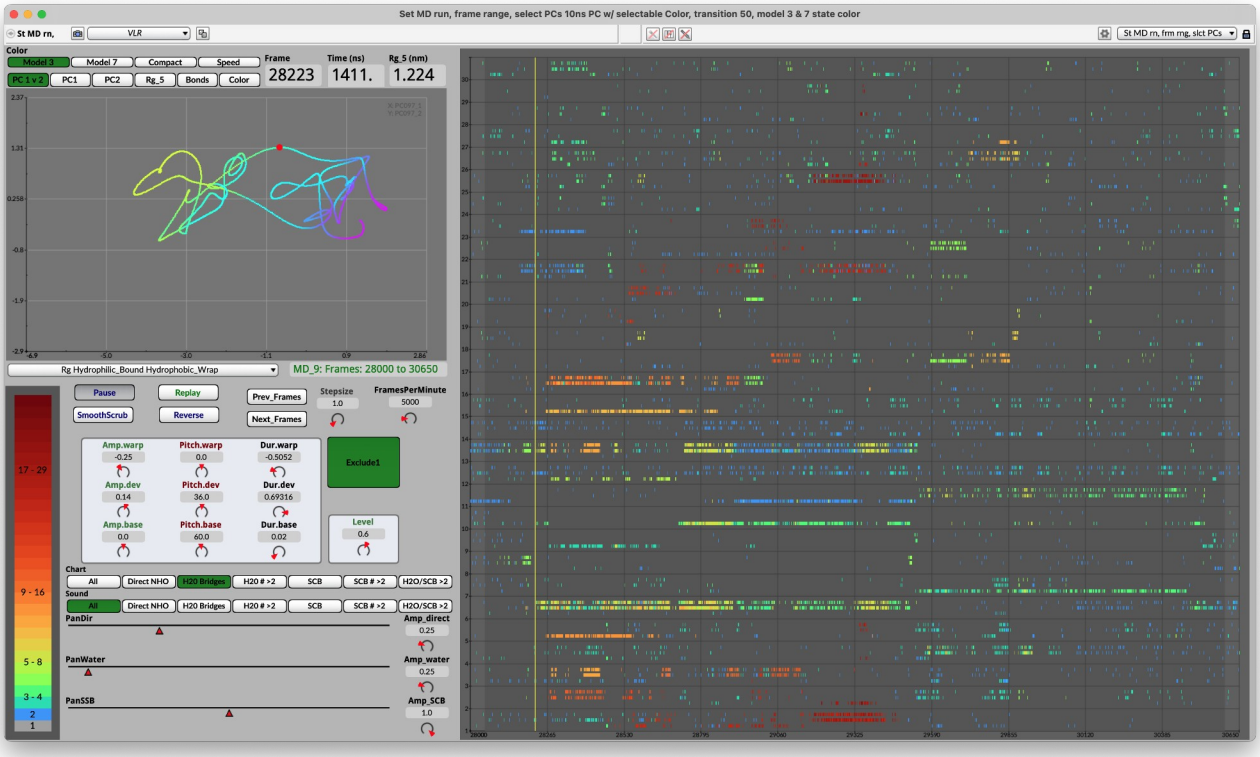

Fig. 2. The sonification/visualization engine for studying polymer collapse. Top left: This window displays two of the PCA components with the largest singular values (PC1 on the horizontal axis and PC2 on the vertical axis); alternatively, it can display individual coordinates as a function of time. Towards the left are globule states (yellow), towards the right are coil states (magenta). The red dot indicates the location of the polymer at the frame/time/R_g displayed above the window; here PNIPAM is undergoing a transition state passage from extended to compact. Right: The 'piano roll' shows the state of WBs (alternatively, DBs or SCBs) as a function of time (horizontal axis) and NIPAM residue (vertical axis); the yellow bar is the time corresponding to the red dot in the C-P space display, when PNIPAM has just lost its water–water HB network and is beginning to form long distance WBs. The color bar on the bottom left codes distance of interactions on the piano roll from local (blue) to highly non-local (dark red) by residue separation along the sequence. Middle left: radio buttons for selecting which bond motifs are displayed on the piano roll and/or heard in the sonification. This makes it possible to follow the reaction coordinate visually and simultaneously follow hydrogen bonding patterns by sound.

Not surprisingly, using only three coordinates — R_g along with either the EPHOA/EPHIA pair or the Wrap/Bound pair — produces a separation between compact and extended polymer states that is nearly equivalent to that produced by the full set of 5 coordinates and covers 95.8% of the variance (SI **Table S5**). This is due to the strong correlation between the two sets of coordinates EPHOA/EPHIA and Wrap/Bound: wrap water preferentially solvates the exposed hydrophobic areas, while bound water solvates the polymer's hydrophilic regions. We note that R_g is not necessary to filter compact from extended states, but adding it as a third coordinate to either the EPHOA/EPHIA pair or to the Wrap/Bound pair of coordinates enhances the separation of states of in the new coordinate system, where PC1 is essentially a measure of compactness, whereas PC2 measures whether a transition state passage along PC1 is dominated by changes in hydrophobic or hydrophilic interactions. Hence we refer to the new coordinate space as C-P space: where the horizontal axis is a measure of C (for

compactness, PC1) and the distance along the vertical axis is *P* (for phobo-philic, PC2). Note that R_g and *C* (PC1) are correlated, whereas *P* (PC2) is not (**SI Fig. S4)**.

For analysis we used a visual/sonification panel to display the transitions in a C-P space based on the PCA of R_g, Wrap water, and Bound water. A sample trajectory of PNIPAM in these coordinates is shown in **Fig. 2** (top left), where compact states are toward the left (yellow), intermediate states are in the center (cyan), and expanded states are toward the right (magenta). The red dot indicates the current position in a transition state passage from right to left (a 10 ns collapse), which is followed by a rapid, 4 ns expansion from left to right.

Visualization and sonification of H-bond patterns. In the piano roll tool (**Fig. 2**), each hydrogen bond or side chain interaction triggers a sonic event called a 'grain' (an impulse response). We map the pitch of each grain to the sequence number (1-30) of the participating residue. This makes it possible to listen to the bonding dynamics in parallel with visually tracking the trajectory of PNIPAM through the C-P state space as it repeatedly collapses and expands.

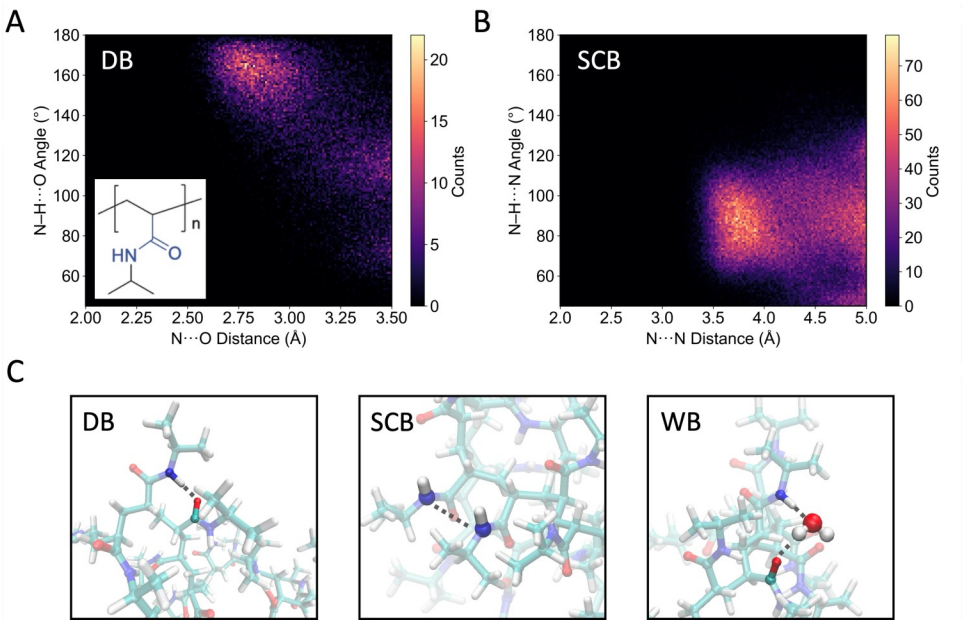

Fig. 3. A. Histogram of direct hydrogen bonds as a function of N...O distance between PNIPAM sidechains and NH...O bond angle. The PNIPAM sidechain is shown in the inset. B. A plot of NHN angle vs. N...N distance between different subunits reveals a marked population near 90° and 3.7 Å; we term this 'side chain bonding' or SCB. C. Examples of direct intersidechain hydrogen bonds (DB), SCB, and water-mediated intersidechain hydrogen bonds (WB).

Our analysis focused on three primary interaction motifs shown in **Fig. 3**: direct PNIPAM–PNIPAM N–H···O H-bonds (DB); water mediated bonds (WB); and sidechain-sidechain NH...N interactions (SCB). The PNIPAM sidechain, shown in **Fig. 3A**, is able to form one intramolecular hydrogen bond: N-H to O=C; linear HNH bonds are not observed. All other H-bonds must be to water molecules. **Fig. 3A** shows a histogram of N...O distance vs. N-H...O angle with the expected maximum at about 2.75 Å and 160°; an example is visualized in **Fig. 3C**. However, PNIPAM can form many more water-bridged hydrogen bonds, an example of which is also shown in **Fig. 3C**. PNIPAM sidechains also interact via another structure, termed here the 'side chain bond' or SCB, which occurs

at an NH...N angle of 90° between different side chains (**Fig. 3B** and **C**). When a series of SCBs forms between adjacent side chains, it can contribute to the long-range organization of the polymer. PNIPAM can also form sidechain-sidechain interactions via two hydrogen bonds bridged by a single water molecule, as seen in Fig. 3C. These WBs greatly outnumber the DBs in all simulations (**Fig. S5**), confirming the observation by Tamai and coworkers,[12] and similar to the importance of water-mediated interactions in protein-protein recognition.[44]

The multimodal nature of the sonification/visualization engine (**Fig. 2** and **Video S1**) made it possible for us to monitor several time-dependent variables in parallel: trajectory through C-P state space, the time evolution of R_g, the non-locality of bonds, and the formation of DB/WB/SCB bonds. Each bonding event is mapped to a sound grain whose pitch is set by the residue (and the contact type within each residue) and whose amplitude and duration are mapped to the number of residues spanned by the bond (the non-locality of the bond); panning across the stereo field helps distinguish DB/WB/SCB, any of which can be selected on or off in different combinations. The tool is highly customizable, with adjustable rate, parameter ranges and perceptual mappings (from log to linear to exponential), allowing each of us to optimize the sound output for analytical focus and auditory acuity. (**Fig. S6**, **S7**, **S8**).

Because bonding events by residue (and the contact type — within each residue) are perceptually separated in pitch space and the auditory stream associated with each H-bond motif is spatially separated by stereo position, we could track multiple bond types in parallel. Furthermore, by monitoring one bond type visually while simultaneously monitoring another bond type aurally, we were able to detect examples of cooperativity during polymer collapse that might otherwise have remained hidden in the data.

As can be best heard in the example in **Video S1**, but also seen in **Fig. 2** (where the red dot in the top left plot marks PNIPAM just entering the transition passage region towards the globule state), formation and loss of compact states is strongly correlated with formation and loss of long-range (residue spacing ≥2) WBs. DBs are frequently bracketed by WBs and can co-exist with WBs on the same residue (**SI Fig. S7**), but their formation rarely correlates with the start of collapse or expansion). SCBs can co-exist or substitute for WBs (**SI Fig. S7**), but they rarely precede collapse of the polymer chain. The excess of longer-distance SCB interactions (**SI Fig. S12**) at mid-range R_g values (~1.22 to 1.5 nm) and the correlation of long distance SCBs with directional shifts in the C-P space trajectories, hints at a possible role for SCBs in hindering transitions or trapping the polymer in intermediate states.

Not all transitions are as fast and direct between globule and coil as the ones shown in **Fig. 2**. For example, **Fig. S8** shows that PNIPAM can get trapped in a very long-lived (>275 ns) state of intermediate compactness, which coincides with long-lived DBs (red), SCBs (green), and WBs (blue) (see **Video S2** and **Video S3**). The ensemble of traps within the middle Gaussian in **Fig. 1C** does not correspond to a single well-defined structural state, but rather a multitude of semi-compact structures whose hydrogen bond pattern hinders further collapse and must be partly dissolved to reach the more compact globule. A cascade of such traps can occur en route from coil to globule resulting in a ‘ball hopping down stairs’ motion of PNIPAM successively lower on the free energy landscape, as in the

example sonified and visualized in **Video S4**. In these extreme cases, PNIPAM contracts gradually in many small steps from globule to coil, rather than in a single highly cooperative step; the reverse stepwise ascending in energy can also occur (see **Video S5**). Large single vs. small multi-step transitions are also evident in **Figs. 1BD**. Contrast these multi-step transitions with a more direct collapse (**Video S6**) and expansion (**Video S7**).

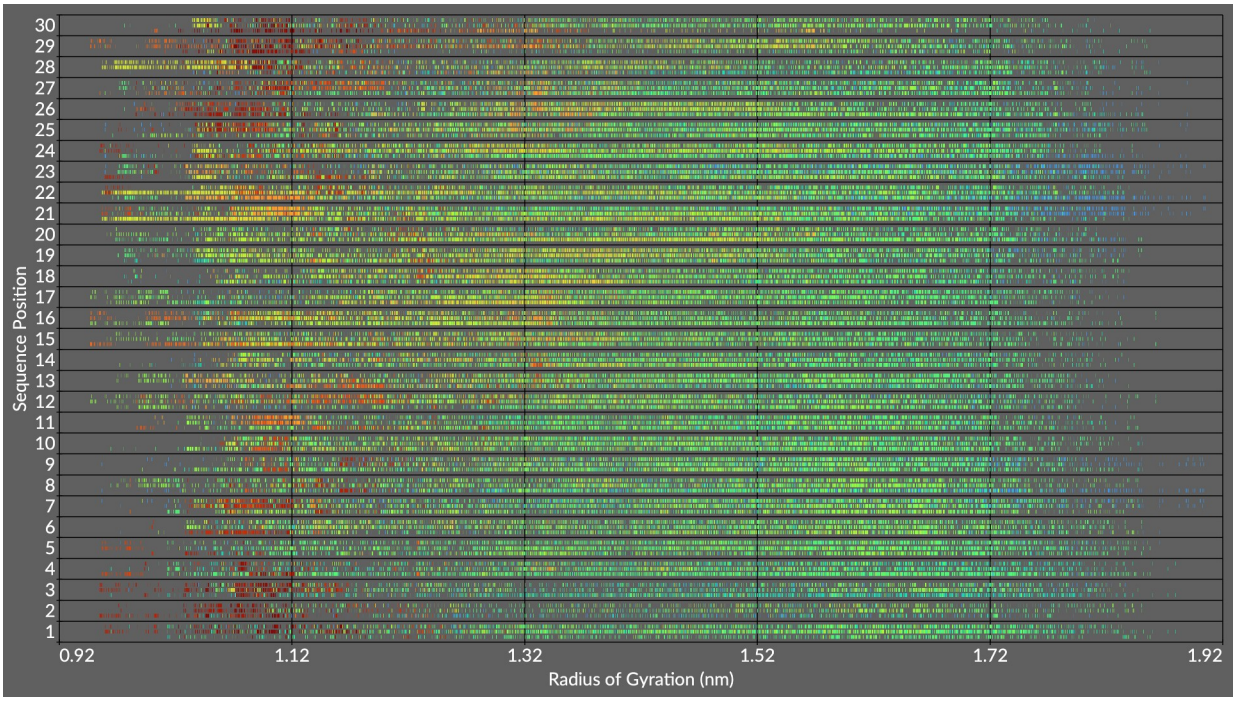

Fig. 4. WBs making greater than 2 side chain contacts along the PNIPAM sequence from 1-30 (vertical axis), as a function of increasing R_g from 0.92 to 1.92 nm (horizontal axis). H-bonds are color- coded from long range (red) to short range (blue). Long range WBs are concentrated between R_g 1.1 to 1.2 nm on the left.

The association of non-local WBs with the compact state is summarized by the histogram in **Fig. 4**, where water-mediated H-bonds are color-coded from long range (red) to short range (blue) and structures have been sorted by R_g from globule (left) to coil (right). Similar plots for all WBs, DBs and SCBs are shown in **SI Figs S10-14**. Long-range water-mediated hydrogen bonds (WBs) are most prevalent in compact structures, and their distribution is similar between center and edge residues, whereas side-chain bonds (SCBs) decrease in prevalence as compactness increases and tend to be concentrated toward the center of the polymer sequence (see **SI Fig. S11**); see also further results below).

Fig. 5 illustrates the local and non-local connectivity of PNIPAM in a globule, intermediate and coil state via a graph network, with numbered NIPAM residues in gray (or green when they form SCBs). Extended states have an extensive network of WBs between adjacent residues, whereas non-local WBs predominantly appear in intermediate and compact states, together with a considerable number of SCBs. Non-local DBs exist, but are relatively rare even in the most compact states. Compared to intermediate states, compact states exhibit a greater number of non-local WBs that also span longer

ranges. Most notably, compact states have many centrally located nodes (centrality is quantified by how often a node lies on a path connecting other node pairs, see Methods).

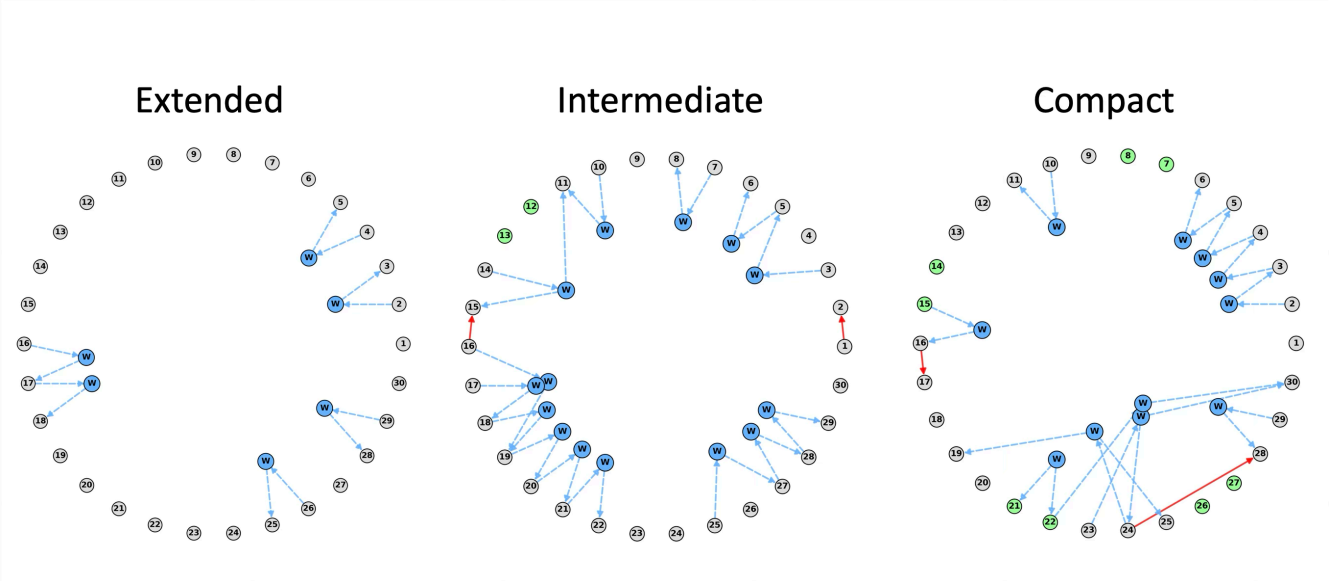

Fig. 5. Representative graphs of a 30-mer PNIPAM chain in extended, intermediate, and compact states (from left to right). PNIPAM residues are shown as nodes numbered from 1 to 30. Edges represent hydrogen bonds, with red solid arrows indicating direct PNIPAM–PNIPAM N–H···O H-bonds (DB), and blue dashed arrows indicating water-mediated H-bonds (WB), where bridging water molecules are shown as blue nodes. Residues involved in side-chain hydrogen bonds (SCB) are highlighted in green. While WB occurs in all three conformational states, long-range DB and WB (connecting non-consecutive residues) predominantly appear in the compact state.

This is further illustrated in **Fig. 6**, where we dig into the role of long-range contacts in driving the coil–globule phase transition. To emphasize distance effects, rather than simply counting WBs and DBs, we weighted each contact by the residue–residue separation $d_{ij}=|i-j|$, where i and j are the connected residues. A higher score reflects longer-range connectivity. Successful transitions are defined by R_g dropping below 1.27 nm (shaded green), whereas failed attempts are shown in red (which may nonetheless yield compact intermediates).

Panel A shows that the success of coil–globule transitions strongly correlates with the distance-weighted contact score of both WBs (blue) and DBs (red). In this excerpt, successful coil-globule transitions are accompanied by a buildup of several non-local WBs, whereas DBs occur mainly after the onset of the transition to compactness (See **Video S8** and **Video S9**). These non-local contacts form paths among PNIPAM residues, leading to centrally located nodes and increased centrality value, which is size-coded in the graph in panel **B.** The centrality value increases rapidly as the oligomers pass from coil through the transition state ensemble into the globule state, while failed attempts (occupation of intermediate states) results in small or no gain in centrality (**Fig. 6C**). Importantly, centrality is not significantly enhanced for residues located in the middle of the sequence: side chains near the periphery are almost as likely to serve as important bridges for long-range H-bond contacts, with the exception of the outermost two NIPAM residues (**Fig. 6D**). This is likely due in part to the symmetry of the molecule, which has twice as many equivalent side chains at the ends as in the middle.

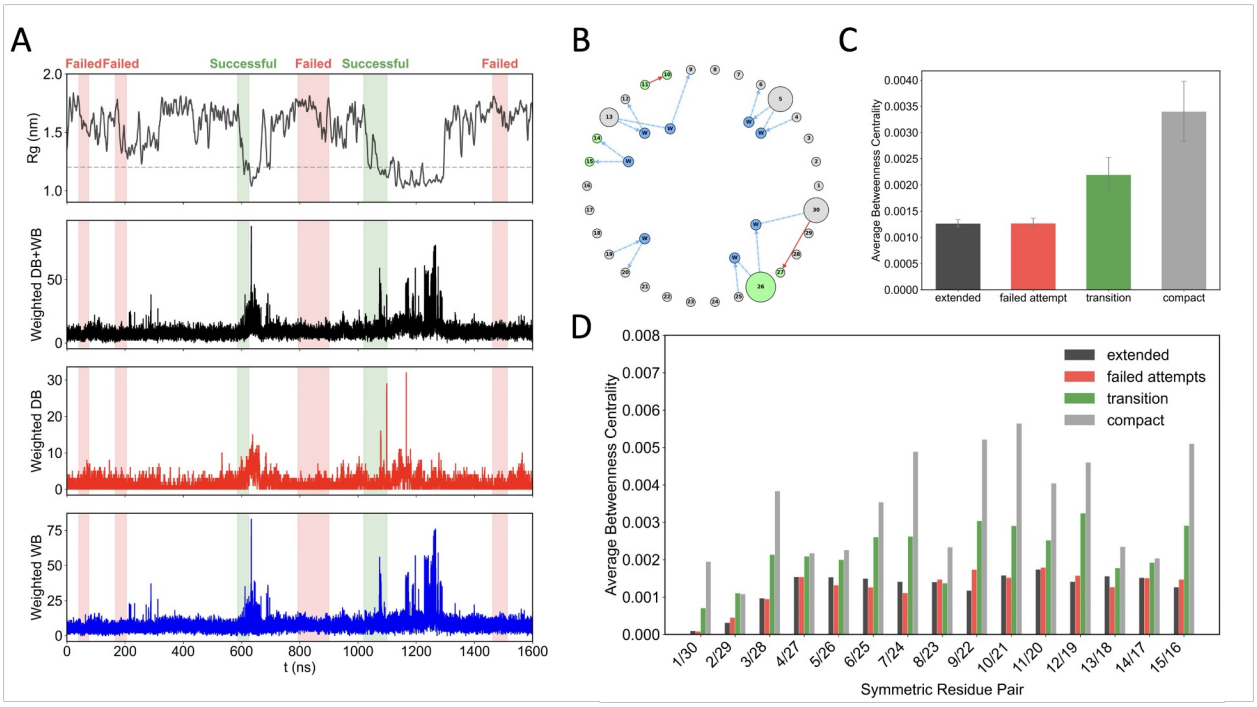

Fig. 6. Long-range contacts play a key role in the PNIPAM globule-coil state transition. (A) Time series from a representative MD trajectory showing (top to bottom): radius of gyration (R_g), total distance-weighted direct (DB) and water-mediated (WB) hydrogen bonds among PNIPAM residues, DB only, and WB only. Transitions are defined here by R_g dropping below 1.27 nm; shaded green for successful transitions, red for failed attempts (that may nonetheless lead to compact intermediates). (B) Graph of a compact PNIPAM state with node size scaled by betweenness centrality, which quantifies how often a node lies on the shortest paths between other node pairs—a proxy for structural connectivity. (C) Average centrality values across states deduced from all eleven MD trajectories: black (extended), red (failed attempt), green (successful transition), gray (compact). Centrality is lowest in extended states and failed attempts, and highest in compact states, with transitions showing intermediate values—highlighting the importance of increased connectivity for successful collapse. (D) Node-resolved centrality values show a broadly uniform distribution across residues, suggesting no localized hotspot governs the transition.

Discussion

Although the importance of hydrophobicity in polymer collapse is well understood, the role of water in aqueous polymer compaction is more active and complex than it is often given credit for, even though it has been pointed out that "water pulls the strings".[45] Our observations indicate that direct, intra-chain hydrogen bonds between amide groups (N-H···O=C) are not the primary structural organizer. Instead, the collapsed globule is organized by a dynamic network of persistent, long distance water bridges, where single water molecules form hydrogen bonds with multiple parts of the polymer chain.

Through a combination of molecular dynamics, auditory analytics, and graph theory, we were able to reveal previously hidden dynamics. We found that the state space of PNIPAM is not a simple "coil-to-globule" picture but includes evidence of highly-populated intermediate states, "traps," and long-lived bonds (DBs, WBs, SCBs) that seem to hinder direct coil-globule transitions. Future directions could include a more detailed characterization of these intermediate states.

The key result is that water-mediated hydrogen bonds assist hydrophobicity as pathfinders for the globule state, as observed also in proteins.[46] DBs occur as well, but play a much smaller role in organization of the compact state. Our observations are in agreement with Yagasaki and Matubayasi,[16] who found that the influence of polymer−polymer hydrogen bonding on compactness is limited. The importance of water-mediated structural interactions has also been highlighted for protein-protein interactions.[44] Thus, to optimize polymer collapse, it is not sufficient to focus solely on tailoring the direct hydrogen bonds: control over water-mediated contacts is mandatory.

Acknowledgements

This work was supported by the Deutsche Forschungsgemeinschaft (DFG, German Research Foundation) under Germany's Excellence Strategy EXC-2033 - 390677874 – RESOLV (WC and MH). MG thanks the Alexander von Humboldt Foundation for support while this work was carried out. W.C. and M.H. also acknowledge support from the Alexander von Humboldt Foundation for a research fellowship under the Henriette-Hertz-Scouting-Program.

References

(1) Haq, M. A.; Su, Y.; Wang, D. Mechanical Properties of PNIPAM Based Hydrogels: A Review. *Materials Science and Engineering: C* **2017**, *70*, 842–855. https://doi.org/10.1016/j.msec.2016.09.081.

(2) Baysal, B. M.; Karasz, F. E. Coil-Globule Collapse in Flexible Macromolecules. *Macro Theory & Simulations* **2003**, *12* (9), 627–646. https://doi.org/10.1002/mats.200350028.

(3) Southall, N. T.; Dill, K. A.; Haymet, A. D. J. A View of the Hydrophobic Effect. *J. Phys. Chem. B* **2002**, *106* (3), 521–533. https://doi.org/10.1021/jp015514e.

(4) Pezzotti, S.; Chen, W.; Novelli, F.; Yu, X.; Hoberg, C.; Havenith, M. Terahertz Calorimetry Spotlights the Role of Water in Biological Processes. *Nat Rev Chem* **2025**, *9* (7), 481–494. https://doi.org/10.1038/s41570-025-00712-8.

(5) Tavagnacco, L.; Zaccarelli, E.; Chiessi, E. Molecular Description of the Coil-to-Globule Transition of Poly(N-Isopropylacrylamide) in Water/Ethanol Mixture at Low Alcohol Concentration. *Journal of Molecular Liquids* **2020**, *297*, 111928. https://doi.org/10.1016/j.molliq.2019.111928.

(6) Pérez-Fuentes, L.; Bastos-González, D.; Faraudo, J.; Drummond, C. Effect of Organic and Inorganic Ions on the Lower Critical Solution Transition and Aggregation of PNIPAM. *Soft Matter* **2018**, *14* (38), 7818–7828. https://doi.org/10.1039/C8SM01679H.

(7) Stetsyshyn, Y.; Ohar, H.; Budkowski, A.; Lazzara, G. Molecular Design and Role of the Dynamic Hydrogen Bonds and Hydrophobic Interactions in Temperature-Switchable Polymers: From Understanding to Applications. *Polymers* **2025**, *17* (11), 1580. https://doi.org/10.3390/polym17111580.

(8) Dalgicdir, C.; Van Der Vegt, N. F. A. Improved Temperature Behavior of PNIPAM in Water with a Modified OPLS Model. *J. Phys. Chem. B* **2019**, *123* (17), 3875–3883. https://doi.org/10.1021/acs.jpcb.9b01644.

(9) Paradossi, G.; Chiessi, E. Solution Behaviour of Poly(N-Isopropylacrylamide) Stereoisomers in Water: A Molecular Dynamics Simulation Study. *Phys. Chem. Chem. Phys.* **2017**, *19* (19), 11892–11903. https://doi.org/10.1039/C7CP00808B.
(10) Tönsing, T.; Oldiges, C. Molecular Dynamic Simulation Study on Structure of Water in Crosslinked Poly(N-Isopropylacrylamide) Hydrogels. *Phys. Chem. Chem. Phys.* **2001**, *3* (24), 5542–5549. https://doi.org/10.1039/b109281m.
(11) Narang, P.; Vepuri, S. B.; Venkatesu, P.; Soliman, M. E. An Unexplored Remarkable PNIPAM-Osmolyte Interaction Study: An Integrated Experimental and Simulation Approach. *Journal of Colloid and Interface Science* **2017**, *504*, 417–428. https://doi.org/10.1016/j.jcis.2017.05.109.
(12) Tamai, Y.; Tanaka, H.; Nakanishi, K. Molecular Dynamics Study of Water in Hydrogels. *Molecular Simulation* **1996**, *16* (4–6), 359–374. https://doi.org/10.1080/08927029608024085.
(13) Tiktopulo, E. I.; Bychkova, V. E.; Ricka, J.; Ptitsyn, O. B. Cooperativity of the Coil-Globule Transition in a Homopolymer: Microcalorimetric Study of Poly(N-Isopropylacrylamide). *Macromolecules* **1994**, *27* (10), 2879–2882. https://doi.org/10.1021/ma00088a031.
(14) Hu, Y.; Buehler, M. J. End-to-End Protein Normal Mode Frequency Predictions Using Language and Graph Models and Application to Sonification. *ACS Nano* **2022**, *16* (12), 20656–20670. https://doi.org/10.1021/acsnano.2c07681.
(15) Scaletti, C.; Rickard, M.; Hebel, K.; Pogorelov, T. V.; Taylor, S.; Gruebele, M. Sonification-Enhanced Lattice Model Animations for Teaching the Protein Folding Reaction. *J. Chem. Ed.* **2022**, *99* (3), 1220–1230. https://doi.org/10.1021/acs.jchemed.1c00857.
(16) Yagasaki, T.; Matubayasi, N. Molecular Dynamics Simulations of Concentrated and Dilute Aqueous Solutions of Poly(*N* -Isopropylacrylamide) Using a Modified OPLS-AA Model. *J. Phys. Chem. B* **2025**, *129* (21), 5234–5244. https://doi.org/10.1021/acs.jpcb.5c00789.
(17) Quoika, P. K.; Kamenik, A. S.; Fernández-Quintero, M. L.; Zacharias, M.; Liedl, K. R. Water Model Determines Thermosensitive and Physicochemical Properties of Poly(N-Isopropylacrylamide) in Molecular Simulations. *Front. Mater.* **2023**, *10*, 1005781. https://doi.org/10.3389/fmats.2023.1005781.
(18) Adroher-Benítez, I.; Moncho-Jordá, A.; Odriozola, G. Conformation Change of an Isotactic Poly (*N* -Isopropylacrylamide) Membrane: Molecular Dynamics. *The Journal of Chemical Physics* **2017**, *146* (19), 194905. https://doi.org/10.1063/1.4983525.
(19) Mochizuki, K.; Sumi, T.; Koga, K. Liquid–Liquid Phase Separation of N-Isopropylpropionamide Aqueous Solutions above the Lower Critical Solution Temperature. *Sci Rep* **2016**, *6* (1), 24657. https://doi.org/10.1038/srep24657.
(20) Berendsen, H. J. C.; Grigera, J. R.; Straatsma, T. P. The Missing Term in Effective Pair Potentials. *J. Phys. Chem.* **1987**, *91* (24), 6269–6271. https://doi.org/10.1021/j100308a038.
(21) Van Der Spoel, D.; Lindahl, E.; Hess, B.; Groenhof, G.; Mark, A. E.; Berendsen, H. J. C. GROMACS: Fast, Flexible, and Free. *J. Comput. Chem.* **2005**, *26* (16), 1701–1718. https://doi.org/10.1002/jcc.20291.
(22) Hess, B.; Bekker, H.; Berendsen, H. J. C.; Fraaije, J. G. E. M. LINCS: A Linear Constraint Solver for Molecular Simulations. *J. Comp. Chem.* **1997**, *18*, 1463–1472.
(23) Miyamoto, S.; Kollman, P. A. Settle: An Analytical Version of the SHAKE and RATTLE Algorithm for Rigid Water Models. *J Comput Chem* **1992**, *13* (8), 952–962. https://doi.org/10.1002/jcc.540130805.
(24) Hoover, W. G. Canonical Dynamics: Equilibrium Phase-Space Distributions. *Phys. Rev. A* **1985**, *31* (3), 1695–1697. https://doi.org/10.1103/PhysRevA.31.1695.
(25) Nosé, S. A Unified Formulation of the Constant Temperature Molecular Dynamics Methods. *J. Chem. Phys.* **1984**, *81* (1), 511–519.

(26) Parrinello, M.; Rahman, A. Crystal Structure and Pair Potentials: A Molecular-Dynamics Study. *Phys. Rev. Lett.* **1980**, *45* (14), 1196–1199. https://doi.org/10.1103/PhysRevLett.45.1196.
(27) Shuang, B.; Cooper, D.; Taylor, J. N.; Kisley, L.; Chen, J.; Wang, W.; Li, C. B.; Komatsuzaki, T.; Landes, C. F. Fast Step Transition and State Identification (STaSI) for Discrete Single-Molecule Data Analysis. *J. Phys. Chem. Lett.* **2014**, *5* (18), 3157–3161. https://doi.org/10.1021/jz501435p.
(28) Samuel Russell, P. P.; Maytin, A. K.; Rickard, M. M.; Russell, M. C.; Pogorelov, T. V.; Gruebele, M. Metastable States in the Hinge-Bending Landscape of an Enzyme in an Atomistic Cytoplasm Simulation. *J. Phys. Chem. Lett.* **2024**, *15* (4), 940–946. https://doi.org/10.1021/acs.jpclett.3c03134.
(29) Mitternacht, S. FreeSASA: An Open Source C Library for Solvent Accessible Surface Area Calculations. *F1000Res* **2016**, *5*, 189. https://doi.org/10.12688/f1000research.7931.1.
(30) Bondi, A. Van Der Waals Volumes and Radii. *J. Phys. Chem.* **1964**, *68* (3), 441–451. https://doi.org/10.1021/j100785a001.
(31) Eisenhaber, F.; Lijnzaad, P.; Argos, P.; Sander, C.; Scharf, M. The Double Cubic Lattice Method: Efficient Approaches to Numerical Integration of Surface Area and Volume and to Dot Surface Contouring of Molecular Assemblies. *J Comput Chem* **1995**, *16* (3), 273–284. https://doi.org/10.1002/jcc.540160303.
(32) Pezzotti, S.; König, B.; Ramos, S.; Schwaab, G.; Havenith, M. Liquid–Liquid Phase Separation? Ask the Water! *J. Phys. Chem. Lett.* **2023**, *14* (6), 1556–1563. https://doi.org/10.1021/acs.jpclett.2c02697.
(33) Pezzotti, S.; Sebastiani, F.; Van Dam, E. P.; Ramos, S.; Conti Nibali, V.; Schwaab, G.; Havenith, M. Spectroscopic Fingerprints of Cavity Formation and Solute Insertion as a Measure of Hydration Entropic Loss and Enthalpic Gain. *Angew Chem Int Ed* **2022**, *61* (29). https://doi.org/10.1002/anie.202203893.
(34) Conti Nibali, V.; Pezzotti, S.; Sebastiani, F.; Galimberti, D. R.; Schwaab, G.; Heyden, M.; Gaigeot, M.-P.; Havenith, M. Wrapping Up Hydrophobic Hydration: Locality Matters. *J. Phys. Chem. Lett.* **2020**, *11* (12), 4809–4816. https://doi.org/10.1021/acs.jpclett.0c00846.
(35) Böhm, F.; Schwaab, G.; Havenith, M. Mapping Hydration Water around Alcohol Chains by THz Calorimetry. *Angew. Chem. Int. Ed.* **2017**, *56* (33), 9981–9985. https://doi.org/10.1002/anie.201612162.
(36) Das Mahanta, D.; Brown, D. R.; Pezzotti, S.; Han, S.; Schwaab, G.; Shell, M. S.; Havenith, M. Local Solvation Structures Govern the Mixing Thermodynamics of Glycerol–Water Solutions. *Chem. Sci.* **2023**, *14* (26), 7381–7392. https://doi.org/10.1039/D3SC00517H.
(37) Scaletti, C.; Hebel, K. J.; Gruebele, M. Auditory Analytics for Pattern Discovery in Protein Folding Dynamics. *Journal of Chemometrics*, in revision **2025**.
(38) Scaletti, C.; Russell, P. P. S.; Hebel, K. J.; Rickard, M. M.; Boob, M.; Danksagmüller, F.; Taylor, S. A.; Pogorelov, T. V.; Gruebele, M. Hydrogen Bonding Heterogeneity Correlates with Protein Folding Transition State Passage Time as Revealed by Data Sonification. *Proc. Natl. Acad. Sci. U.S.A.* **2024**, *121* (22), e2319094121. https://doi.org/10.1073/pnas.2319094121.
(39) Scaletti, C. Computer Music Languages, Kyma, and the Future. *Computer Music Journal* **2002**, *26* (4), 69–82. https://doi.org/10.1162/014892602320991392.
(40) *OpenSmalltalk*. OpenSmalltalk. https://opensmalltalk.org (accessed 2025-06-03).
(41) Tavagnacco, L.; Zaccarelli, E.; Chiessi, E. Modeling Solution Behavior of Poly(*N* -Isopropylacrylamide): A Comparison between Water Models. *J. Phys. Chem. B* **2022**, *126* (20), 3778–3788. https://doi.org/10.1021/acs.jpcb.2c00637.

(42) Krieger, F.; Fierz, B.; Bieri, O.; Drewello, M.; Kiefhaber, T. Dynamics of Unfolded Polypeptide Chains as Model for the Earliest Steps in Protein Folding. *Journal of Molecular Biology* **2003**, *332* (1), 265–274. https://doi.org/10.1016/S0022-2836(03)00892-1.
(43) Hummer, G. From Transition Paths to Transition States and Rate Coefficients. *The Journal of Chemical Physics* **2004**, *120* (2), 516–523. https://doi.org/10.1063/1.1630572.
(44) Papoian, G. A.; Ulander, J.; Wolynes, P. G. Role of Water Mediated Interactions in Protein−Protein Recognition Landscapes. *J. Am. Chem. Soc.* **2003**, *125* (30), 9170–9178. https://doi.org/10.1021/ja034729u.
(45) Hummer, G. Water Pulls the Strings in Hydrophobic Polymer Collapse. *Proc. Natl. Acad. Sci. U.S.A.* **2007**, *104* (38), 14883–14884. https://doi.org/10.1073/pnas.0706633104.
(46) Levy, Y.; Onuchic, J. N. Water and Proteins: A Love–Hate Relationship. *Proc. Natl. Acad. Sci. U.S.A.* **2004**, *101* (10), 3325–3326. https://doi.org/10.1073/pnas.0400157101.